Tampere University

Timo Hartikainen

DESIGN AND IMPLEMENTATION OF A WET THERMAL OXIDATION OVEN AND APPLICATION TO FABRICATION OF VCSELS

Bachelor of Science thesis
Faculty of Engineering and Natural Sciences
Examiners: Assoc. Prof. Tapio Niemi and
Kostiantyn Nechay
May 2021

ABSTRACT

Timo Hartikainen: Design and Implementation of a Wet Thermal Oxidation Oven and Application to Fabrication of VCSELs
Bachelor of Science thesis
Tampere University
Bachelor's Degree Program in Science and Engineering
May 2021

The purpose of this thesis was to design and implement a wet thermal oxidation oven optimized for the fabrication of vertical-cavity surface-emitting lasers (VCSEL). An oxide aperture created by the lateral oxidation of a VCSEL structure plays an important role in the operation of the device. It creates a current aperture that enables the confinement of carriers and photons within a small active region to emit light. The diameter and symmetry of the oxide aperture must be adjusted precisely in order to meet the requirements defined by the electro-optical characteristics of the device.

This work investigated the oxidation processes of semiconductor materials and the working principle of a wet thermal oxidation oven. Based on the research, the wet thermal oxidation oven built in this work included a quartz process chamber, an IR heating element and a dedicated water vapor production system. Samples were placed on a graphite carrier which absorbed and distributed the radiation of the heating element. The temperature of the carrier was measured with a Pt100 resistance thermometer, and the temperature of the sample was measured directly with an IR pyrometer. The power of the heating element was regulated by a PID temperature controller. All process parameters were controlled by automated computer software in order to increase run-to-run reproducibility.

The most important control parameters of an oxidation oven were found to be sample temperature, carrier gas flow rate, water vapor concentration and oxidation time. Also, the position and orientation of the sample in a process chamber may have a great effect on the oxidation result. The accuracy of the process can be improved significantly with an integrated in-situ monitoring system.

As a result of the work, the uniformity of the lateral oxidation depth across macro samples (with a typical size of several centimeters) has reached values lower than $\pm 0.5\,\mu m$. Also, an excellent symmetry of the oxide apertures has been achieved. Oxidized VCSEL structures were successfully processed into well-functioning single-emitters operating in single mode, which is considered to be an untrivial task, especially without integrating expensive in-situ monitoring into the system.

The future development of the oxidation oven will focus on adding an in-situ monitoring capability to the system, which will increase the reliability and output quality of the process. Another improvement will be increasing the size of the sample in order to use the system in a commercial manufacturing process.

Keywords: wet thermal oxidation, oxidation oven, VCSEL, oxide aperture

TIIVISTELMÄ

Timo Hartikainen: Termisen märkäoksidointiuunin suunnittelu ja rakentaminen ja sen soveltaminen VCSEL:ien valmistukseen
Kandidaatintyö
Tampereen yliopisto
Teknis-luonnontieteellinen tutkinto-ohjelma
Toukokuu 2021

Tämän kandidaatintyön tarkoituksena oli suunnitella ja rakentaa terminen märkäoksidointiuuni, joka soveltuisi erityisesti pinnasta emittoivien lasereiden (VCSEL) valmistukseen. VCSEL:n rakenteen lateraalisella oksidoinnilla tuotetulla oksidiaukolla on tärkeä rooli laitteen toiminnassa. Se luo virta-aukon, joka mahdollistaa varauksenkuljettajien ja fotonien keskittämisen pieneen aktiiviseen alueeseen valon tuottamiseksi. Oksidiaukon halkaisijaa ja symmetriaa täytyy säädellä tarkasti, jotta VCSEL:n elektro-optisten ominaisuuksien määrittelemät vaatimukset voidaan täyttää.

Työssä selvitettiin puolijohteiden oksidointiprosesseja ja oksidointiuunien toimintaperiaate. Selvityksen perusteella rakennettiin terminen märkäoksidointiuuni, joka pohjautui kvartsilasista valmistettuun prosessikammioon, infrapunalämpöelementtiin ja erikoistuneeseen vesihöyryntuottojärjestelmään. Näytteet asetettiin grafiittialustalle, joka absorboi ja levitti lämpöelementin säteilyä. Alustan lämpötilaa mitattiin Pt100-vastuslämpötila-anturilla, ja näytteen lämpötilaa mitattiin suoraan pyrometrillä. Lämpöelementin tehoa ohjattiin PID-lämpötilasäätimellä. Kaikkia prosessiparametreja säädettiin automatisoidulla tietokoneohjelmalla toistettavuuden parantamiseksi.

Työssä havaittiin, että oksidointiuunin tärkeimmät prosessiparametrit ovat seuraavat: näytteen lämpötila, kantokaasun virtausnopeus, vesihöyrykonsentraatio ja oksidointiaika. Lisäksi näytteen sijainnilla ja suuntautumisella prosessikammiossa voi olla suuri vaikutus oksidointitulokseen. Prosessin tarkkuutta on mahdollista lisätä huomattavasti integroidulla in-situ-seurantajärjestelmällä.

Työn tuloksena lateraalisen oksidointisyvyyden vaihtelu makronäytteissä (tyypillisesti useiden senttimetrien kokoisia) saavutti arvoja alle $\pm 0.5\,\mu\text{m}$. Lisäksi saavutettiin erinomainen oksidiaukkojen symmetria. Oksidoidut VCSEL-rakenteet prosessoitiin onnistuneesti yhdessä optisessa muodossa laseroiviksi yksittäisemittereiksi, mitä pidetään haastavana tehtävänä erityisesti ilman kallista integroitua in-situ-seurantajärjestelmää.

Oksidointiuunin jatkokehitys tulee keskittymään in-situ-seurantajärjestelmän lisäämiseen, mikä lisää prosessin luotettavuutta ja tuloksen laatua. Toinen parannus tulee olemaan näytekoon kasvattaminen, jotta järjestelmää on mahdollista käyttää kaupallisessa valmistusprosessissa.

Avainsanat: terminen märkäoksidointi, oksidointuuni, VCSEL, oksidiaukko

PREFACE

This thesis was made as a part of bachelor's degree program in Science and Engineering at Tampere University. The practical work was performed in Modulight, Inc. mainly during the summer of 2020.

I would like to warmly thank the examiners of the work Tapio Niemi and Kostiantyn Nechay for the valuable feedback and mentorship received during the writing process. The practical part of the work was conducted under the guidance of Kostiantyn Nechay who taught me a lot about the topic and beyond, provided detailed help in practical experiments and was always easily approachable.

Tampere, 16th May 2021

Timo Hartikainen

CONTENTS

LIST OF SYMBOLS AND ABBREVIATIONS

3D	Three-Dimensional Space
CCD	Charge-Coupled Device
CVD	Chemical Vapor Deposition
DBR	Distributed Bragg Reflector
DIC	Differential Interference Contrast
FWHM	Full Width At Half-Maximum
IBS	Ion-Beam Sputtering
IC	Integrated Circuit
IR	Infrared
LiDAR	Light Detection And Ranging
PECVD	Plasma-Enhanced Chemical Vapor Deposition
PID	Proportional–Integral–Derivative
SEM	Scanning Electron Microscope
TEOS	Tetraethyl Orthosilicate
VCSEL	Vertical Cavity Surface Emitting Laser

1 INTRODUCTION

The discovery of quantum mechanics at the beginning of the 20th century greatly broadened our understanding of the principles of solid-state matter. This led to numerous breakthroughs in solid-state physics, one of them being the discovery of semiconductor materials. Particularly, semiconductors and their oxides have become important compounds in many fields of science and technology.

Lasers are optical devices capable of emitting coherent and monochromatic light, and many types of them are based on semiconductors. A vertical-cavity surface-emitting laser (VCSEL) is an important type of semiconductor laser that is processed in a wet thermal oxidation oven in order to incorporate a semiconductor oxide layer in its structure during manufacturing.

This work consists of two different parts. The first part is a literature survey that describes the theoretical model of wet thermal oxidation of semiconductors and existing wet thermal oxidation ovens. The second part consists of designing and implementing a new wet thermal oxidation oven optimized for the fabrication of VCSELs.

The oxidation processes of semiconductor materials and oxide apertures for VCSELs are discussed as background information in Chapter 2. Chapter 3 presents the basic working principle of a wet thermal oxidation oven. The design and implementation of the new wet thermal oxidation oven are described in Chapter 4. The performance of the new wet thermal oxidation oven is analyzed in Chapter 5. The conclusions of the work can be found in Chapter 6 along with suggestions for future work and research.

2 BACKGROUND

Semiconductors can be classified as a group of materials whose electrical conductivity lies in-between the values of conductors and insulators. Elemental semiconductors can be found in the group IV of the periodic table (e.g. Si and Ge). Binary semiconductor compounds are produced by mixing elements in the groups III and V (e.g. AlAs, GaAs and InP), the groups II and VI (e.g. ZnS, ZnSe and CdS) or the groups IV and VI (e.g. PbS, PbSe, and PbTe). In addition, ternary (e.g. $Al_xGa_{1-x}As$, $GaAs_{1-x}P_x$ and $Hg_{1-x}Cd_xTe$), quaternary (e.g. $Ga_xIn_{1-x}As_yP_{1-y}$) and other types of semiconductors exist. [1]

One of the most peculiar features of semiconductors is the possibility to precisely tailor their electrical and optical properties by utilizing different semiconductor compounds and their elemental ratio. As a result, semiconductor technology has found usage in countless amount of commercial and industrial applications and has become the backbone of modern technological progress. In particular, modern electronics fully rely on semiconductors: integrated circuits (IC) and their building blocks, diodes and transistors, are conventionally silicon-based, while optoelectronics and photonics field often extends to the exploitation of GaAs- and InP-based materials, e.g. for laser diode fabrication. Because of their crystalline structure, semiconductor compounds demand epitaxial deposition techniques to manufacture thin-film structures that appear in electronic and optoelectronic devices. Upon crystal growth, semiconductor structures undergo numerous processing steps, such as etching, metalization and oxidation, depending on the final purpose. This work describes oxidation processes that are critical to many semiconductor processing workflows.

2.1 Oxidation processes of semiconductor materials

Oxidation is the chemical reaction that can be characterized by the loss of electrons, while reduction is the reverse reaction defined by the gain of electrons. In other terms, the oxidation reaction may be also defined by oxidation states: oxidation is an increase in the oxidation state of an atom, ion or compound, opposite to the reduction which is a decrease in the oxidation state of an atom, ion or compound. The component increasing its oxidation state is called a reductant and the component decreasing its oxidation state is called an oxidant. Together, oxidation and reduction represent a redox reaction which is

the transfer of electrons from a reductant to an oxidant. The oxidation reaction is named after oxygen (O_2) which is the most common oxidant.

Oxides are chemical compounds that contain oxygen and can be abundantly found in nature in many forms. Oxides play an important role in many fields of technology, mainly due to the altered properties of oxidized materials compared to their unoxidized counterparts. Oxides may serve different purposes: in electronics, they are often used as insulators, while in photonics, oxides are often employed in waveguides and optical coatings because of their low refractive indices.

In ambient conditions, oxidation reactions obey a self-limiting behavior. Oxides produced in these conditions are called native oxides. For example, pure silicon exposed to air will grow a silicon dioxide (SiO_2) layer with a thickness of ~2 nm. [2] Native oxide thickness for pure aluminum is ~4 nm [3]. Typically, native oxide thicknesses are less than applications incorporating oxide layers require [2]. To achieve larger thicknesses, conventionally, two main fabrication methods of oxide layers are used: thermal oxidation and oxide deposition. These methods are described in the following sections by the example of silicon dioxide which is a very common oxide in the semiconductor industry. These generalized methods may be extended to other semiconductors as well.

2.1.1 Thermal oxidation

Thermal oxidation process is done at high temperatures in either a dry environment containing high oxygen content or a wet environment containing high humidity. Thus, two subprocesses are distinguished: dry thermal oxidation and wet thermal oxidation.

Dry thermal oxidation is a type of oxidation in which silicon reacts with pure oxygen atmosphere:

$$\mathrm{Si} + \mathrm{O_2} \xrightarrow{1000-1200\ ^\circ\mathrm{C}} \mathrm{SiO_2}.$$

A stable and thin oxide layer, typically with a thickness of hundreds of nanometers, can be formed when conducting the process at a lower temperature of around 800 °C. In dry thermal oxidation, oxide growth is slow, however, it results in high-density oxide layers offering high breakdown voltage preferable for electronics applications. [4]

In the wet thermal oxidation, silicon reacts with the water vapor which is present in the process environment. The reaction is given by:

$$\mathrm{Si} + 2\,\mathrm{H_2O} \xrightarrow{900-1000\ ^\circ\mathrm{C}} \mathrm{SiO_2} + 2\,\mathrm{H_2}.$$

Wet thermal oxidation can be characterized as a much faster process; on the other hand, it results in inferior oxide quality when compared to the dry thermal oxidation [4]. The comparison of the oxide growth rates is presented in Table 2.1.

Table 2.1. *Oxide growth rates of wet and dry oxidation of silicon [4].*

Temperature (℃)	Dry oxidation ($nm\,h^{-1}$)	Wet oxidation ($nm\,h^{-1}$)
900	19	100
1000	50	400
1100	120	630

While oxidation speed is highly dependent on the method of choice and the process temperatures, the oxidation rate is not linear and highest at the beginning, since the already created oxide layer at the surface will prevent oxygen atoms from reacting with the silicon crystal beneath. [5]

2.1.2 Oxidation by vapor deposition

If a silicon surface is covered by other films or if silicon oxide has to be created on a non-silicon surface, the silicon oxide layer may be deposited in this case. Silicon dioxide can be deposited by several different processes and source gases. Several deposition techniques may be employed for the oxide deposition: e-beam coating, ion-beam sputtering (IBS), chemical vapor deposition (CVD), etc. CVD is one of the most common deposition methods which involves the chemical reaction of the gaseous precursors (e.g. Si and O_2).

For instance, silane (SiH_4) pyrolysis takes advantage of heat for cleaving the reactants. The quality of the silicon dioxide produced by this method is low. [4] The reaction is as follows:

$$SiH_4 + 4\,NH_3 \xrightarrow{400\ ℃} SiO_2 + 2\,H_2.$$

On the other hand, TEOS ($Si(OC_2H_5)_4$) produces a very pure silicon dioxide film with high electric strength when conducting the process under a vacuum [4]. TEOS is cleaved at high temperatures as follows:

$$Si(OC_2H_5)_4 \xrightarrow{750\ ℃} SiO_2 + \text{byproducts}.$$

The pressure and temperature of the process are critical for the quality and uniformity of the deposited oxide layers [4].

Plasma-enhanced chemical vapor deposition (PECVD) involves the plasma of the reacting gases, which allows using lower deposition temperatures than in thermal chemical vapor deposition [4]. Such deposition method avoids defect formation in the underlying silicon substrate, as well as, dopant diffusion and degradation of the metal layers [6]. On the other hand, PECVD-prepared silicon dioxide films may have higher impurity concentration (e.g. hydrogen, nitrogen, H_2O and Si-OH groups) and porosity [7].

2.1.3 Deal–Grove model

The growth of a thick oxide layer on a material is described mathematically by the Deal-Grove model published by Bruce Deal and Andrew Grove in 1965 [5]. The model was published after the observations made in the 1960s that the oxidation rate of silicon followed first a linear and then a parabolic dependency. The model is still widely used for predicting the oxidation rate of silicon and other semiconductors, such as AlAs [8].

The oxidation process of a semiconductor is divided into three phases:

1. The oxidant travels from the bulk of the oxidizing gas to the outer surface of the sample.
2. The oxidant is transferred across the oxide film towards the semiconductor.
3. The oxidant reacts with the semiconductor.

The phases and mathematical symbols used in the following calculations are displayed in Figure 2.1.

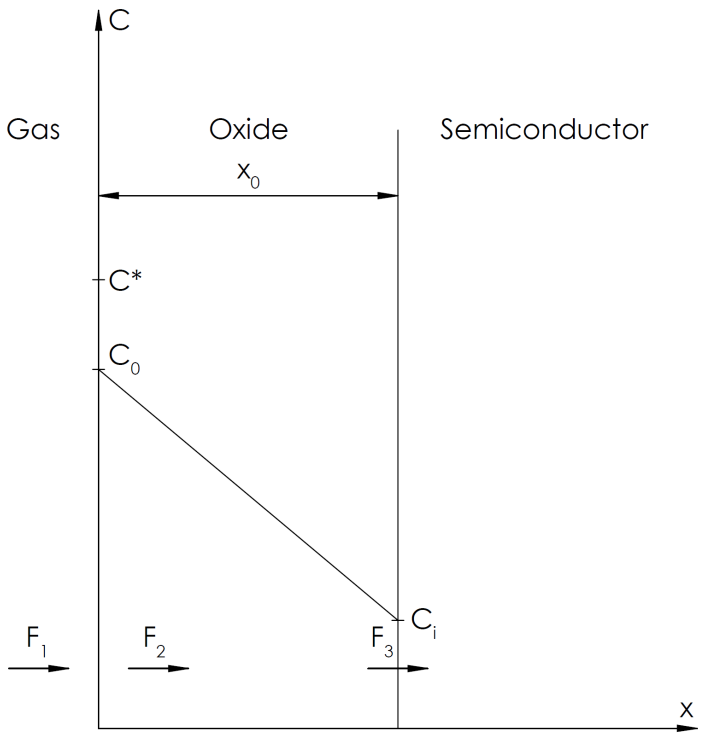

Figure 2.1. *Model for the oxidation of a semiconductor [5].*

It holds for the flux of the oxidant from the gas to the vicinity of the outer surface of the sample

$$F_1 = h(C^* - C_0), \tag{2.1}$$

where h is a gas-phase transport coefficient, C_0 is the concentration of the oxidant at the outer surface of the oxide at any given time and C^* is the equilibrium concentration of the

oxidant in the oxide.

The equilibrium concentration of the oxidant is related to the partial pressure of the oxidant in the gas according to Henry's law

$$C_* = K_H p, \tag{2.2}$$

where K_H is Henry's law constant and p is the partial pressure of the oxidant in the gas.

The flux of the oxidant across the oxide layer is described by Fick's law

$$F_2 = -D_{eff}\frac{C_0 - C_i}{x_0}, \tag{2.3}$$

where D_{eff} is the effective diffusion coefficient, C_i is the concentration of the oxidant near the oxide-semiconductor interface and x_0 is the thickness of the oxide layer.

The flux at the oxidation front is given by

$$F_3 = -kC_i, \tag{2.4}$$

where k is a reaction rate constant related to the oxide-semiconductor interface.

Assuming a steady state, it holds that $F_1 = F_2$ and $F_2 = F_3$. By solving C_i and C_0 and applying the limit where the diffusivity becomes very small compared to the reaction rate contants associated with the surfaces, k and h, $C_i \to 0$ and $C_0 \to C^*$. As a result, the flux $F = F_1 = F_2 = F_3$ becomes

$$F = \frac{kC^*}{1 + k/h + kx_0/D_{eff}}. \tag{2.5}$$

A differential equation describing the rate of the growth of the oxide layer can be derived from the equation (2.5) as follows

$$\frac{dx_0}{dt} = \frac{F}{N} = \frac{kC^*/N}{1 + k/h + kx_0/D_{eff}}, \tag{2.6}$$

where N is the number of oxidant molecules incorporated into a unit volume of the oxide layer.

The initial condition for this step is set to take into account an initial layer of oxide x_i that might have been present on the semiconductor prior to the oxidation step under consideration:

$$x_0 = x_i \text{ at } t = 0. \tag{2.7}$$

Applying the initial condition (2.7), the solution of the differential equation (2.6) becomes

$$x_0^2 + Ax_0 = B(t + \tau), \tag{2.8}$$

where

$$A = 2D_{eff}(1/k + 1/h), \tag{2.9}$$

$$B = 2D_{eff}C^*/N, \tag{2.10}$$

and

$$\tau = (x_i^2 + Ax_i)/B. \tag{2.11}$$

The oxide thickness as a function of time is solved from the quadratic equation (2.8) as follows

$$x_0(t) = \frac{A}{2}\left[\left(1 + \frac{t+\tau}{A^2/4B}\right)^{\frac{1}{2}} - 1\right]. \tag{2.12}$$

Examining the two limiting forms of the equation (2.12), two general results can be written:

1. For relatively small oxidation times ($t + \tau << A^2/4B$), the equation (2.12) produces a linear law:

$$x_0 = \frac{B}{A}(t + \tau), \tag{2.13}$$

where the relation

$$\frac{B}{A} = \frac{kh}{k+h}\left(\frac{C^*}{N}\right) \tag{2.14}$$

is referred to as the linear rate constant.

2. For relatively large oxidation times ($t >> A^2/4B$), a parabolic law applies:

$$x_0^2 = Bt, \tag{2.15}$$

where the coefficient B is referred to as the parabolic rate constant.

A, B and τ are physicochemical constants characteristic to a certain material and temperature. τ corresponds to a shift in the time coordinate which accounts for the presence of the initial oxide layer x_i. The values of the constants for wet oxidation of silicon are presented in Table 2.2.

Table 2.2. *Rate constants for oxidation of silicon in wet oxygen (95 °C H_2O) [5].*

Oxidation temperature (°C)	A (µm)	B (µm^2 h^{-1})	B/A (µm h^{-1})	τ (h)
920	0,50	0,203	0,406	0
1000	0,226	0,287	1,27	0
1100	0,11	0,510	4,64	0
1200	0,05	0,720	14,40	0

The lower the oxidation temperature is, the longer the oxidation will be linear with respect to time [9]. To maintain controlled oxidation, it's beneficial to stay in the linear region when oxidating tens to hundreds of nanometers. In case of AlAs, a favorable oxidation environment depends both on the sample temperature and aluminum concentration. [8]

2.2 Oxide apertured VCSELs

A vertical-cavity surface-emitting laser (VCSEL) belongs to the semiconductor diode laser family and emits light perpendicularly to the growth plane. VCSELs typically produce narrow linewidth emission (~0,5 nm FWHM) with lower temperature sensitivity and high beam quality, especially, when compared to the conventional edge-emitting lasers [10]. VCSELs have found numerous applications in industrial and commercial fields, such as high-speed optical data communication, laser printing, LiDAR and 3D sensing, etc.

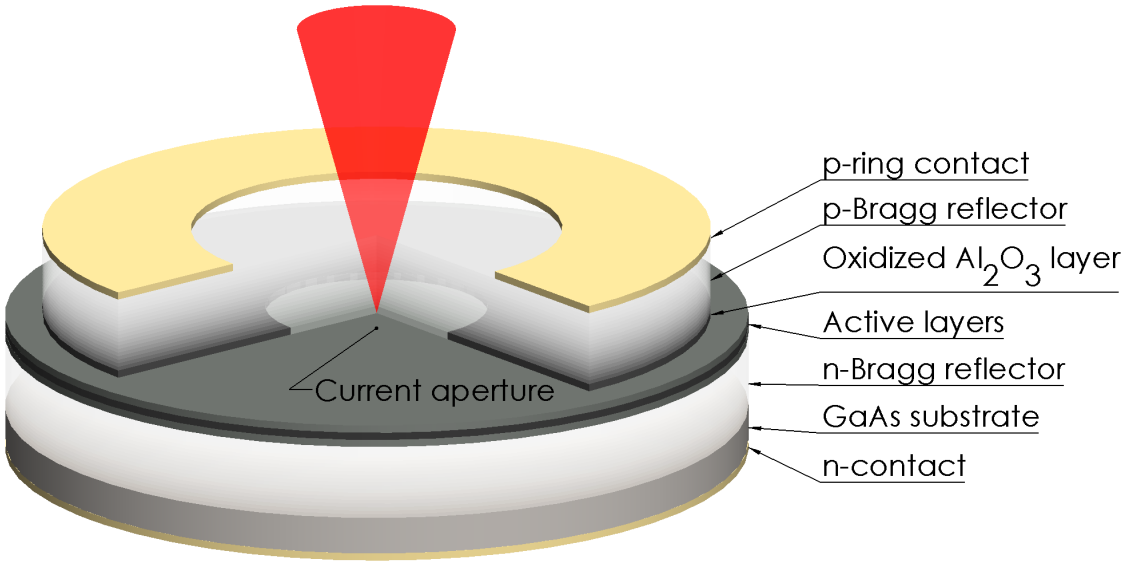

Figure 2.2. *Schematic cross-sectional view of a VCSEL [11].*

Figure 2.2 illustrates the general layer structure of a VCSEL. This structure is epitaxially grown on an n-GaAs substrate, where a circular mesa is formed by means of etching of the top distributed Bragg reflector (DBR). Conventionally, the diameter of the mesa is a couple of tens of micrometers. In this particular VCSEL architecture, AlAs layer with high

Al content (typ. 97–98 %) and with a typical thickness of several tens of nanometers is epitaxially grown on top of the active region, prior to the top-Bragg reflector deposition. This layer has the highest Al content within the whole structure and is meant for wet thermal oxidation in the device processing chain following mesa etching. [11] The lateral oxidation of this layer creates a current aperture which enables the confinement of carriers and photons within a small active region [12]. In the reaction, AlAs is oxidized into Al_2O_3 [10]:

$$2\,AlAs + 6\,H_2O \xrightarrow{400\ ^\circ C} Al_2O_3 + 2\,AsO_3 + 6\,H_2.$$

Oxidation rate is approximately $1\,\mu m\,min^{-1}$ in a water vapour atmosphere which is heated up to 400 °C [11]. During device fabrication, the oxides are often unstable, which may result in delamination, for instance, after rapid thermal annealing where structure undergoes rapid heating above 350 °C [13].

Figure 2.3 outlines the oxide aperture in a scanning electron microscope (SEM) image of a VCSEL mesa cleaved along the diameter. The oxide layer and the direction of the oxidation are shown by the arrows. Also, the oxidation gradient of the different layers of the top DBR is observed. A minor upward crack in the mesa may have originated either from the cleaving of the mesa or strain produced by the oxidation.

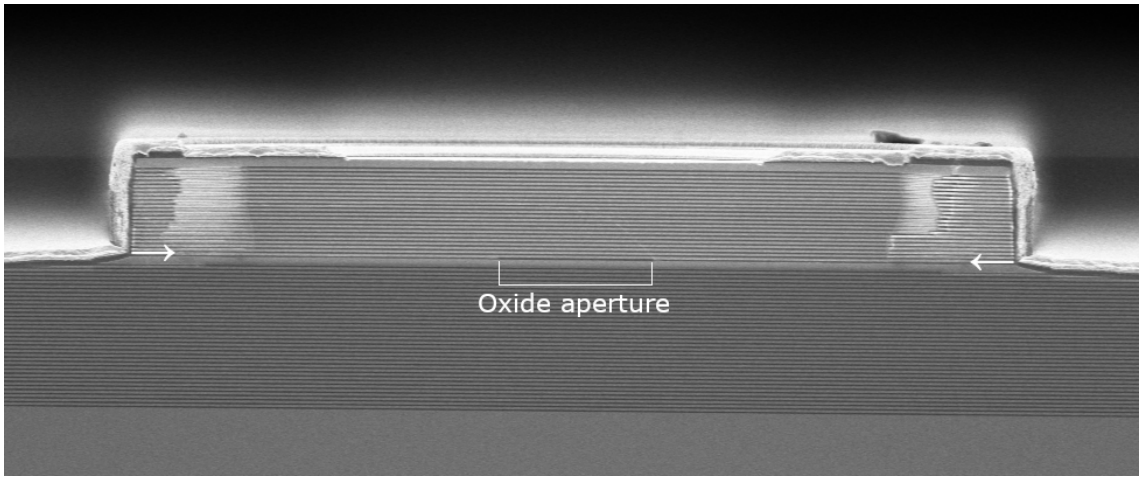

Figure 2.3. *A cross-section scanning electron microscope image of a VCSEL.*

The previously mentioned reaction can be slowed down by adding Ga into AlAs up to several percents. The reaction becomes: [10]

$$2\,Al_xGa_{1-x}As + 6\,H_2O \xrightarrow{400\ ^\circ C} (Al_xGa_{1-x})_2O_3 + As_2O_3 + 6\,H_2.$$

Water delivery into the process chamber can be implemented by means of any inert gas, such as nitrogen (N_2) or argon (Ar). An inert gas must be used to keep hydrogen unreacted. The presence of hydrogen removes the excessive amount of arsenic in order to produce a high-quality oxide layer in a controlled manner. Any active gas, such as

oxygen which reacts with hydrogen to form water, stops the oxidation process completely. [10]

Although the aforementioned reaction produces small amounts of arsine (AsH_3) in the exhaust as a result of hydrogen reacting with arsenic, typically, the safety concerns over arsine toxicity are not risen considering its negligible amounts. [10]

3 WORKING PRINCIPLE

Wet thermal oxidation process can be done at high temperatures in an environment containing high humidity. Conventionally, the prerequisites are achieved using a bubbler vessel filled with heated deionized water and a heated process chamber. The majority of devices work under atmospheric pressure to avoid expensive vacuum equipment. Water is heated slightly below the boiling point (e.g. 85 – 95 °C) and an inert carrier gas, such as nitrogen, is used to deliver water vapor into the process chamber. The process chamber is usually a sufficiently long tube (e.g. 0,5 – 1,5 m) in order to maintain a laminar water vapor flow. Conventionally, it is manufactured either from metal or glass. The tube is heated evenly upon reaching the process temperature, and a sample is placed in the middle of it. Figure 3.1 illustrates the general design of a wet thermal oxidation oven. [10]

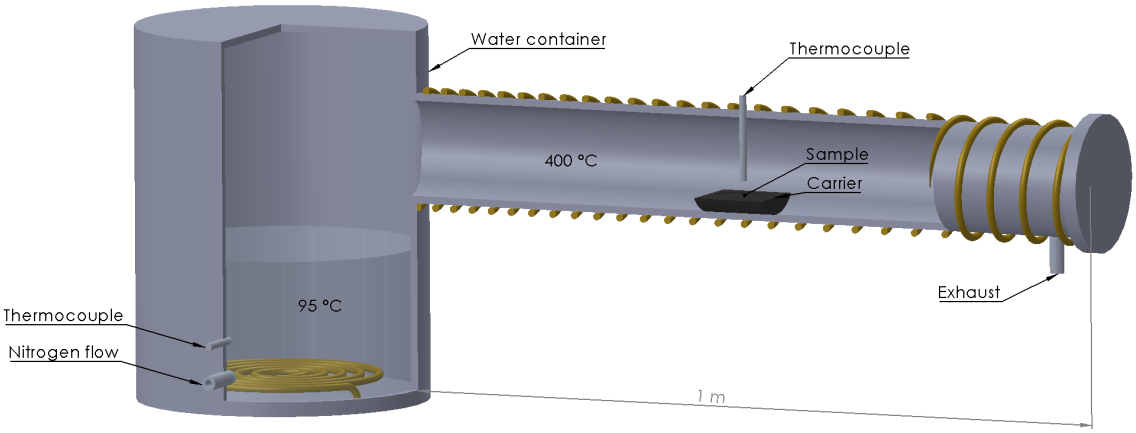

Figure 3.1. *Schematic design of a wet thermal oxidation oven [10].*

On the other hand, wet thermal oxidation ovens can be constructed to operate under a vacuum. A vacuum atmosphere increases the controllability of the process by eliminating sources of contamination, removing heat convections and decreasing oxidation rate.

3.1 Control parameters

Typically, the primary output parameter of interest in the wet thermal oxidation is the resulting lateral oxidation depth. The secondary output parameters of the wet thermal oxidation may include oxidation isotropy, which is needed to create round apertures, long-

range oxidation depth uniformity and reproducibility. The aforementioned process outputs are defined both by the material properties and process parameters. This work aims at adjusting the process parameters under the fixed material properties. The controllable wet thermal oxidation process parameters are:

1. sample temperature
2. nitrogen flow rate
3. water temperature
4. sample orientation and position in the chamber
5. oxidation time.

The sample temperature is the most crucial parameter when it comes to oxidation rate and uniformity. Therefore, the temperature must be monitored and adjusted accurately, preferably with one degree of accuracy. This is possible to achieve by placing multiple thermocouples as close as possible to the sample and dividing the process chamber into multiple heating zones. [10]

The nitrogen flow rate can be monitored and adjusted easily either by a mass flow meter or a mass flow controller. A sufficient flow rate depends on the process chamber size but, according to multiple research results [14, 15], there exists a critical flow rate for each water temperature. Above the critical value, the oxidation rate is independent of the nitrogen flow rate. Typically, the flow rate is 1–3 $\mathrm{l\,min^{-1}}$. Nitrogen can be heated up before entering the bubbler vessel but this does not affect the result if water volume is large enough. [10]

Water vapor concentration is adjusted accurately by controlling the carrier gas flow rate. As a consequence, the water temperature is kept sufficiently below the boiling point to avoid extensive vapor production and overpressure. It has been observed that 85 °C is enough to keep the carrier gas flow rate sufficiently low. [10]

As gas flow distribution in the process chamber is almost impossible to predict, usually, it is approximated to be constant in a large enough volume around the sample. Even temperature and water vapor distribution can be adjusted by changing the place of the sample in the chamber and tilting it towards the vapor flow. As well, different sample carrier materials may affect the temperature distribution. [10]

The oxidation time must be chosen so that desired oxidation depth is achieved. It depends vastly on the equipment and other process parameters. [10]

3.2 Oxidation depth assessment

The oxidation depth defines the size of the oxide aperture which is responsible for the current and field confinement. Thus, the oxidation depth must be adjusted precisely to meet the requirements of the oxide aperture which in turn defines the electro-optical characteristics of the VCSEL. Oxide depth assessment can be performed either in the post-processing measurements or using real-time in-situ monitoring. The oxidation depth can be measured either directly from the mesas or from other parts of the mask layout.

The oxide layer is visible in optical microscopes equipped with a Nomarski prism and a CCD camera. The Nomarski prism increases contrast in a transparent sample using differential interference contrast (DIC) microscopy. The CCD camera is used to capture infrared light which passes the DBR of the mesa. Viewing efficiency and contrast depends on the illumination wavelength, the depth of the oxide layer and the composition of the layer above it. A sufficient magnification in our tests was from 10X to 100X.

Alternatively, a cross-section scanning electron microscope (SEM) image can be taken from the mesas cleaved along the diameter. Compared to the optical microscope assessment, this method gives information about oxidation depth distribution in the mesa, particularly, the oxidation gradient of the different layers of the top DBR. However, it's difficult to perform the method for small-sized mesas and the cleaving may impact the measurement.

Yet another approach is to use a focused ion beam to remove layers either from the side or the top of the mesa or oxidize test samples that lack the top DBR. This approach allows very accurate results but is slow.

The most straightforward way of in-situ monitoring is based on the direct viewing of the oxidizing pattern using a CCD camera. This method requires an appropriate viewport in the furnace for the camera. [16] Other challenges include withstanding the heat produced by the furnace and the short operating distances of the magnification objectives required in the system.

Another in-situ monitoring approach is based on measuring the average change of the VCSEL wafer reflectivity over a large area of patterns. The approach works with uniform replicated patterns on the wafer. [17]

3.3 State-of-the-art systems

The market has commercial products both for conventional silicon wafer processing and in particular VCSEL manufacturing. The dedicated solutions can be found from several companies, and selected systems from AET Technologies, California Scientific and Koyo Thermo Systems will be introduced in the following.

ALOX is a furnace from AET Technologies designed for the wet thermal oxidation of III-V compound semiconductors on wafers up to 6". It operates under a vacuum and maintains oxidation temperatures from 350 °C to 600 °C. Real-time in-situ monitoring allows automatic oxide aperture diameter control. The reported standard deviation of the oxide aperture diameter is less than 0.45 µm on a 6" wafer and run-to-run deviation less than 0.05 µm. The furnace is showed in Figure 3.2. [18]

Figure 3.2. *ALOX wet thermal oxidation furnace by AET Technologies [18].*

California Scientific's VIXEL-320 atmospheric-pressure wet thermal oxidation system is intended for the fabrication of VCSELs on wafers up to 6". The integrated in-situ monitoring has good visibility of the oxide front through a thin optical window which is possible due to the atmospheric pressure. VIXEL-320 has oxidation temperature range from 430 °C to 500 °C and oxidation uniformity ± 1.0 µm on a 6" wafer. The system is presented in Figure 3.3. [19]

Figure 3.3. *VIXEL-320 wet thermal oxidation furnace by California Scientific [19].*

Koyo Thermo Systems has established its VF-3000 vertical furnace for the low-temperature wet thermal oxidation process of the AlAs layer in VCSELs. The furnace can process 4" to 8" wafers in up to 75-wafer-sized baches. VF-3000 is pictured in Figure 3.4. [20]

Figure 3.4. *VF-3000 vertical furnace by Koyo Thermo Systems [20].*

Commercial oxidation furnaces are very costly, and most of the scientific publications on wet thermal oxidation exploit custom-built oxidation furnaces. These furnaces have featured various technologies, such as vertical vapor deposition, rotating samples, precision evaporators and IR pyrometers [21, 22].

4 DESIGN AND IMPLEMENTATION

This chapter describes the design and implementation of the wet thermal oxidation oven constructed in this work. The most important requirement was the best possible control of the process parameters, especially sample temperature and water vapor concentration. Also, the oxidation oven was designed to support an in-situ monitoring system and up to 6" wafers. Additionally, the automation of the process was prioritized.

The oxidation oven was built based on a quartz tube, an IR heating element and a dedicated vapor production system. Other main parts included an IR pyrometer and temperature controllers. The process parameters of the oxidation oven were controlled by computer software allowing fully automated operation after sample loading. The design of the oxidation oven is pictured in Figure 4.1.

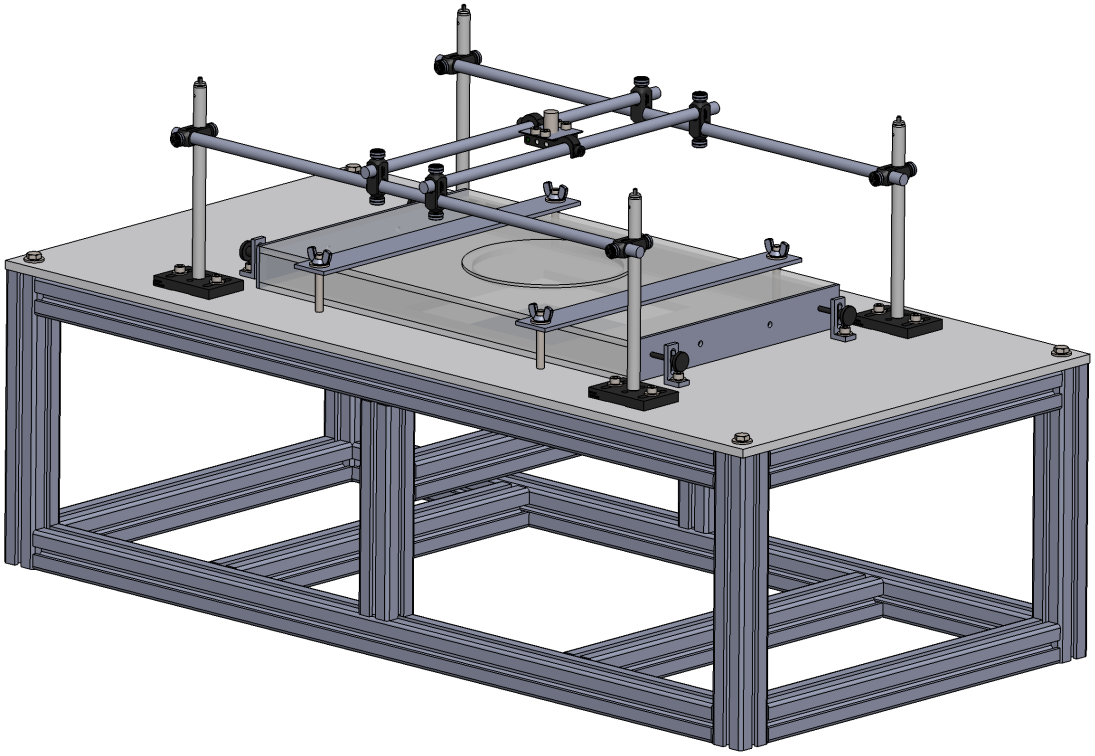

Figure 4.1. *The design of the oxidation oven.*

Figure 4.2 labels the different parts of the oxidation oven. Vapor inlets and outlets were connected with pipes to an evaporator and an exhaust line, respectively.

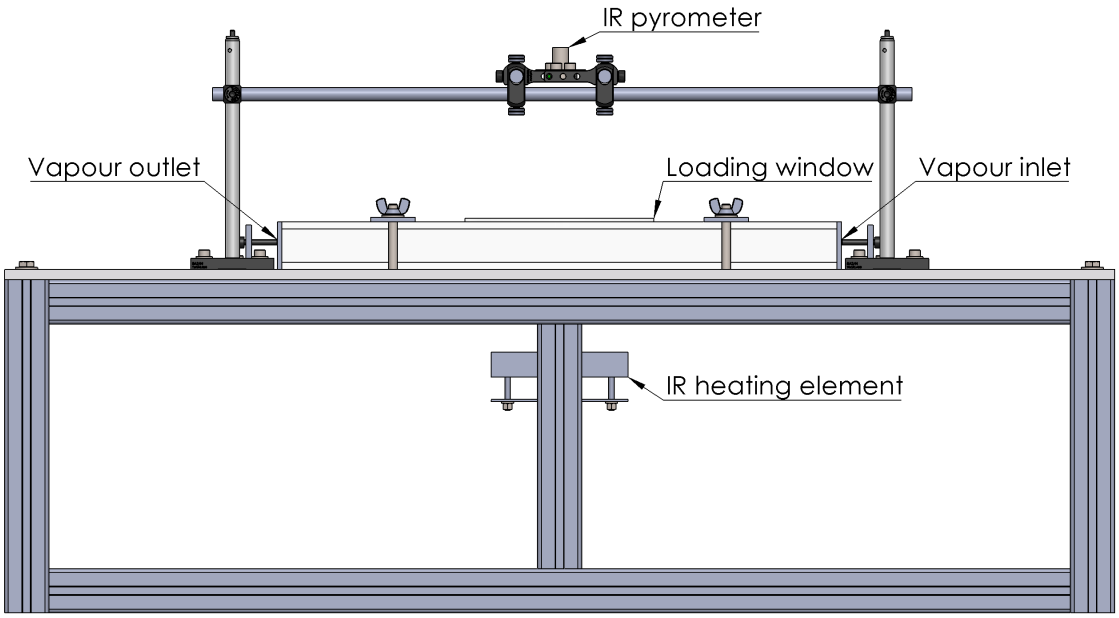

Figure 4.2. *The parts of the oxidation oven.*

The metal frame of the oxidation oven was constructed from aluminum extrusion profile which allowed easy mounting for many components. The top surface of the frame was covered with a cement board resistant to high temperatures and humidity.

The system was placed in a laminar flow hood. This provided a clean environment for handling samples even if the oxidation oven wasn't located in a cleanroom due to excessive heat generation.

4.1 Process environment

The process environment of the oxidation oven was a quartz tube designed and built specifically for the purpose. As there weren't available any ready-made quartz tubes with the shape and dimensions necessary, a custom tube had to be manufactured from multiple quartz sheets. The tube is illustrated in Figure 4.3.

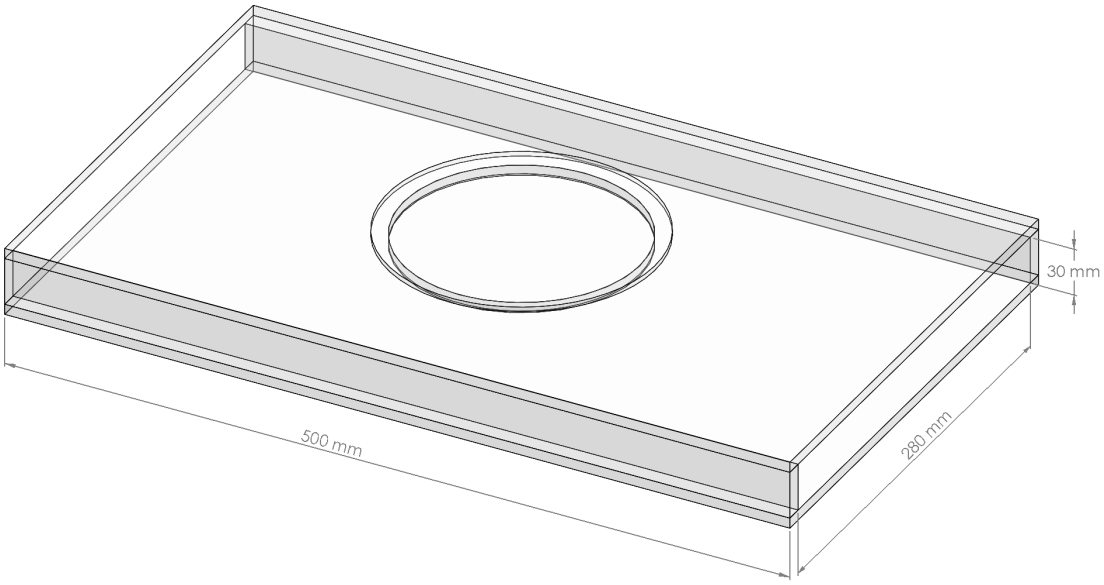

Figure 4.3. *The quartz tube of the oxidation oven.*

The quartz tube was manufactured from Heraeus Quarzglas HSQ300 quartz glass. The material has very high purity and optical transmission as well as high temperature stability and thermal shock resistance [23]. The optical transmission of HSQ300 is plotted in Figure 4.4.

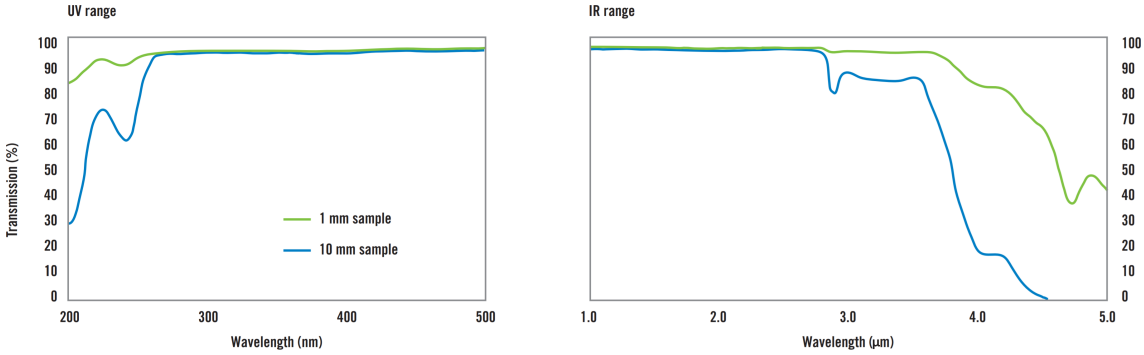

Figure 4.4. *The optical transmission of HSQ300 quartz glass [23].*

The quartz tube was equipped with a loading window which was situated directly above a sample carrier. The window was polished from both sides in order to provide a clear view for the IR pyrometer. Oxidation samples were placed on the carrier and removed from it through the loading window using tweezers or a vacuum wand.

In order to avoid the use of any sealant materials, all quartz surfaces touching each other had a matte finish which provided a good sealing. The quartz tube was sealed with aluminum covers in both ends. The sealing of this interface was implemented using a fiberglass ribbon. The covers contained inlets and outlets for the water vapor and a pass-through hole for a temperature sensor wire.

The modular construction of the tube was held together by clamping the tube to the sur-

face of the table. Also, the tube was pushed together from both ends, which often provided enough rigidity alone. The modular construction of the tube was very convenient for maintenance purposes, such as placing and removing the sample carrier which was bigger than the loading window.

4.2 Temperature control

The oxidation samples were placed on a graphite carrier that lied at the bottom of the quartz tube. The carrier was made of graphite in order to absorb most of the heat radiation. In addition, graphite has excellent heat conductivity. A Pt100 resistance thermometer attached to the carrier allowed measuring the temperature of the carrier and the sample accurately.

The sample carrier was heated through the quartz tube by a 1000 W infrared quartz heating element which was positioned under the tube. The aluminum profile frame allowed flexible positioning of the heater. The useful wavelength range of the heater was 1,5–8 µm which was transmitted efficiently by the quartz tube directly to the sample carrier. The mean surface temperature of the heater at full power was approximately 770 °C.

The heater was controlled by a PID temperature controller which measured the sample carrier temperature. The controller had the precision of one decimal place in setting and measuring the temperature. Another safety temperature controller was used in order to interrupt the power of the heater if the maximum carrier temperature would have been exceeded.

The temperature of the sample was monitored also directly using the IR pyrometer mounted on an optical post. The post allowed moving the pyrometer to measure different points of the sample.

4.3 Vapor production

The water vapor used in the oxidation process was produced in a dedicated vaporization system which allowed very precise control over the characteristics of the vapor. The system consisted of three main instruments which are displayed in Figure 4.5:

1. a liquid flow meter
2. a mass flow controller
3. an evaporator.

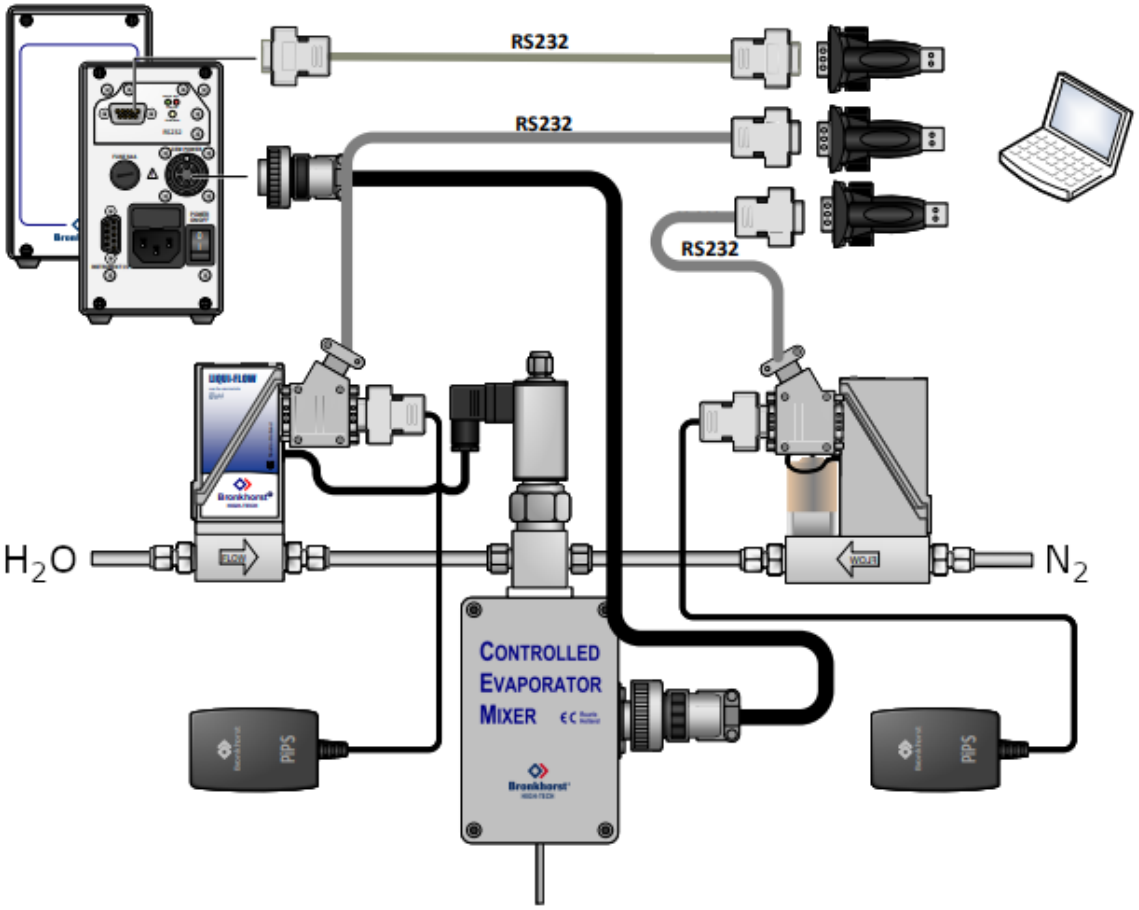

Figure 4.5. *The hook-up diagram of the water vaporization system.*

The liquid flow meter measured the flow of water from a distilled water line to the evaporator. A purging valve installed in the vicinity of the liquid flow meter allowed replacing old water in pipes before running the oxidation process. The flow of water could be adjusted from 2 to 120 $\mathrm{g\,h^{-1}}$.

The flow of nitrogen used as the carrier gas was measured and controlled by the mass flow controller. The supported flow range of the mass flow controller was 0,2–10 $\mathrm{l\,min^{-1}}$.

The evaporator unit was equipped with a valve in order to control the distilled water flow. The maximum temperature of the vapor produced was 200 °C. The vapor was then mixed with the carrier gas and supplied to the process chamber.

The vapor mixture was supplied to the process chamber using insulated Teflon pipes. The Teflon pipes suited well for the purpose because of their high working temperature of 260 °C.

After the process chamber, the vapor was directed to an exhaust line through a condenser. The condenser was equipped with a tap at the bottom for draining out the water condensation. Eventually, the exhaust gases were directed outdoors using an adjustable ventilation flow.

5 PERFORMANCE

The wet thermal oxidation oven constructed and described in the previous chapter was tuned and evaluated in a series of tests. Test samples included VCSEL mesas of three different diameters arranged both as single-emitters and arrays. The oxidized material was AlGaAs. The tuning of the oxidation oven focused on achieving the best possible lateral oxidation depth uniformity and oxide aperture symmetry in different sample shapes, sizes and structures. In this work, an experimental and qualitative approach in the analysis of the results was emphasized. An in-depth quantitative analysis of the performance will be conducted based on a larger set of test results available in a future work.

The oxidation of the mesas was observable already in the first test, which was a positive indication of the proper general functioning of the system and allowed rapid proceeding to the fine-tuning and optimization of the process parameters. The control parameters listed in Section 3.1 were altered one by one keeping everything else constant in order to determine their optimal values. Figure 5.1 shows the comparison of an undeveloped early-stage oxidation process and the developed oxidation process at the end of this work.

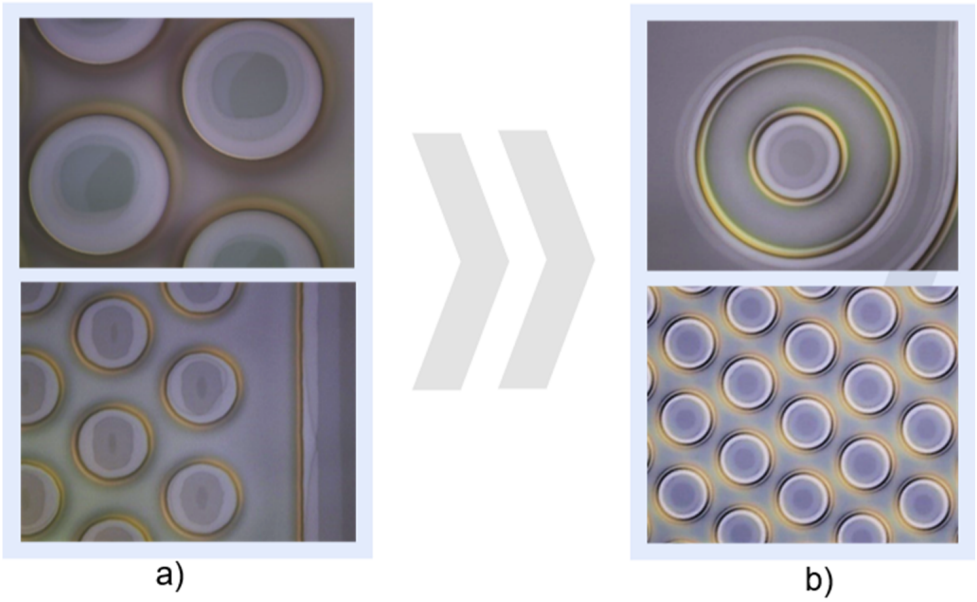

Figure 5.1. *Microscope photographs of oxidized VCSEL mesas. a) Undeveloped process with very high oxidation ununiformity and asymmetry. b) Developed process resulting in uniform lateral oxidation depth and oxide aperture symmetry across large processing pieces. [24]*

The effect of the parameters on the process was observed to follow the behaviors described in Section 3.1. Carrier gas flow rate and water vapor concentration had the most effect on the uniformity and symmetry of the oxidation. The oxidation temperature was fixed at 420 °C. The nitrogen flow rate was tuned to 2 $\mathrm{l\,min^{-1}}$ with the water flow rate set to 10 $\mathrm{g\,h^{-1}}$. The arrangement produced an average oxidation rate of $0.5\,\mu\mathrm{m\,min^{-1}}$, which aligns with predictions based on the Deal-Grove model in similar conditions [25, 26].

Oxidated samples were analyzed using an optical microscope equipped with a Nomarski prism and a CCD camera. The lateral oxidation depth of the mesas was calculated by determining the pixel count ratio of the diameter of the oxide aperture and the diameter of the mesa. Figure 5.2 illustrates one ratio of the diameters used in this work.

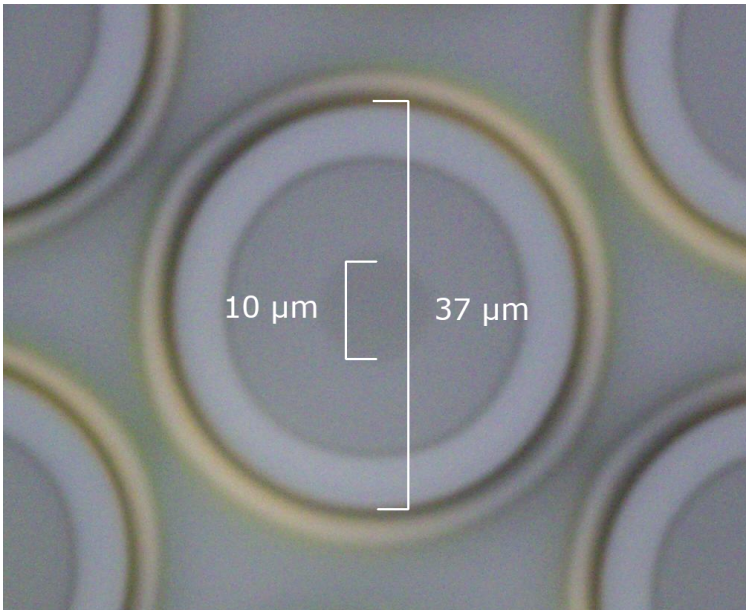

Figure 5.2. *A microscope photograph of an oxidized VCSEL mesa that has a diameter of* $37\,\mu\mathrm{m}$*. The lateral oxidation depth is* $13.5\,\mu\mathrm{m}$*, and the diameter of the oxide aperture is* $10\,\mu\mathrm{m}$*.*

The lighter outer ring of the mesa in Figure 5.2 is caused by the oxidation of the top DBR. The darker inner ring of the mesa is the oxidation of the oxide layer. The different oxidizing layers are shown in a cross-section SEM image in Figure 2.3.

By the end of this work, the uniformity of the lateral oxidation depth across macro samples (with a typical size of several centimeters) has reached values lower than $\pm 0.5\,\mu\mathrm{m}$. In comparison, the lateral oxidation depth uniformity of California Scientific's VIXEL-320 is $\pm 1.0\,\mu\mathrm{m}$ on a 6" wafer [19]. The standard deviation of the oxide aperture diameter of AET Technologies' ALOX is reported as less than $0.45\,\mu\mathrm{m}$ on a 6" wafer [18]. In addition, an excellent symmetry of the oxide apertures was achieved in this work. The oxidized structures were successfully processed into well-functioning VCSEL single-emitters operating in single mode. [24]

6 CONCLUSIONS

This work focused on designing and implementing a wet thermal oxidation oven optimized for the fabrication of VCSELs. VCSELs require very accurate, uniform and symmetric lateral oxidation of their structure. Commercial oxidation systems have been developed but they tend to be highly expensive and uncustomizable.

The literature survey revealed that the oxidation of semiconductor materials is a complex process and many control parameters are required in order to achieve high-quality results. In the development process, the following process parameters were considered: sample temperature, nitrogen flow rate, water vapor concentration, sample orientation and position in the chamber and oxidation time.

The oxidation oven developed in this work has demonstrated the ability to perform a highly controllable and reproducible wet thermal oxidation process that provides excellent uniformity and symmetry of oxide aperture. The ability to precisely control the water concentration and flow of the nitrogen carrier while maintaining a uniform temperature distribution across the whole sample has made it possible to achieve single-mode operation in VCSEL single-emitters, which is considered to be an untrivial task, especially without integrating expensive in-situ monitoring into the system.

The future work will address the challenge of adding an in-situ monitoring capability to the system. The challenge is produced by the hot environment and the short working distance of magnification objectives required in the system. The current quartz chamber used is already suited for the short working distance but it doesn't provide sufficient heat insulation. The in-situ monitoring will allow even more precise oxidation depth control. Also, it will reduce testing time and material as new oxidation processes are developed and different VCSEL structures are used.

Another improvement will be scaling up the oxidation oven to support a wider range of wafer sizes and the automatization of the process. High lateral oxidation depth uniformity across large wafers and low run-to-run deviation will enable the oxidation oven to be used in a commercial manufacturing process.

REFERENCES

[1] Yacobi, B. *Semiconductor Materials An Introduction to Basic Principles*. eng. 1st ed. 2003. Microdevices, Physics and Fabrication Technologies. New York, NY: Springer US, 1–3. ISBN: 0-306-47942-7.

[2] Bohling, C. and Sigmund, W. Self-Limitation of Native Oxides Explained. *Silicon* 8.3 (July 2016), 339–343. ISSN: 1876-9918. DOI: 10.1007/s12633-015-9366-8. URL: https://doi.org/10.1007/s12633-015-9366-8.

[3] Evertsson, J., Bertram, F., Zhang, F., Rullik, L., Merte, L., Shipilin, M., Soldemo, M., Ahmadi, S., Vinogradov, N., Carla, F., Weissenrieder, J., Göthelid, M., Pan, J., Mikkelsen, A., Nilsson, J.-O. and Lundgren, E. The thickness of native oxides on aluminum alloys and single crystals. *Applied Surface Science* 349 (May 2015), 826–832. DOI: 10.1016/j.apsusc.2015.05.043.

[4] *Philipp Laube, Semiconductor Technology*. Cited 28.2.2021. URL: https://www.halbleiter.org/en.

[5] Deal, B. E. and Grove, A. S. General Relationship for the Thermal Oxidation of Silicon. *Journal of Applied Physics* 36.12 (1965), 3770–3778. DOI: 10.1063/1.1713945. eprint: https://doi.org/10.1063/1.1713945. URL: https://doi.org/10.1063/1.1713945.

[6] Meysam, Z., Ahangarani, S. and Maryam, Z. Properties of Silicon Dioxide Film Deposited By PECVD at Low Temperature/Pressure. *Metallurgical and Materials Engineering* 20 (July 2014), 89–96. DOI: 10.5937/metmateng1402089M.

[7] Fernandez-Lima, F., Rodriguez, J., Pedrero, E., Filho], H. [, Llovera, A., Riera, M., Dominguez, C., Behar, M. and Zawislak, F. Ion beam analysis of PECVD silicon oxide thin films. *Nuclear Instruments and Methods in Physics Research Section B: Beam Interactions with Materials and Atoms* 243.1 (2006), 200–204. ISSN: 0168-583X. DOI: https://doi.org/10.1016/j.nimb.2005.07.244. URL: http://www.sciencedirect.com/science/article/pii/S0168583X05016447.

[8] Baca, A. and Ashby, C. Fabrication of GaAs Devices. Jan. 2005. ISBN: 9780863413537. DOI: 10.1049/PBEP006E.

[9] Legay, P., Caillet, F., Decobert, J., Leprince, L., Le Roux, G. and Quillec, M. Oxide confining layer on an InP substrate. *Journal of Applied Physics* 85.4 (1999), 2428–2430. DOI: 10.1063/1.369561. eprint: https://doi.org/10.1063/1.369561. URL: https://doi.org/10.1063/1.369561.

[10] Saarinen, M. Wet Thermal Oxidation of $Al_xGa_{1-x}As$ structures and Application to Fabrication of Resonance Devices. (1999).

[11] Michalzik, R. *VCSELs: Fundamentals, Technology and Applications of Vertical-Cavity Surface-Emitting Lasers*. Springer Series in Optical Sciences. Springer Berlin Heidelberg, 2012. ISBN: 9783642249860. URL: https://books.google.fi/books?id=1-y5BQAAQBAJ.

[12] Arai, M., Nishiyama, N., Shinada, S., Koyama, F. and Iga, K. AlAs Oxidation System with H2O Vaporizer for Oxide-Confined Surface Emitting Lasers. *Japanese Journal of Applied Physics* 39.Part 1, No. 6A (June 2000), 3468–3469. DOI: 10.1143/jjap.39.3468. URL: https://doi.org/10.1143%2Fjjap.39.3468.

[13] Jia, H., Wang, W., Wang, W., Li, W., Huang, Q., Zhou, J. and Xue, Q. Improved thermal stability of wet-oxidized AlAs. *Applied Physics Letters* 80 (Feb. 2002), 974–976. DOI: 10.1063/1.1448166.

[14] Choquette, K. D., Geib, K. M., Ashby, C. I. H., Twesten, R. D., Blum, O., Hou, H. Q., Follstaedt, D. M., Hammons, B. E., Mathes, D. and Hull, R. Advances in selective wet oxidation of AlGaAs alloys. *IEEE Journal of Selected Topics in Quantum Electronics* 3.3 (1997), 916–926.

[15] Geib, K. M., Choquette, K. D., Hou, H. Q. and Hammons, B. E. Fabrication issues of oxide-confined VCSELs. *Vertical-Cavity Surface-Emitting Lasers*. Ed. by K. D. Choquette and D. G. Deppe. Vol. 3003. International Society for Optics and Photonics. SPIE, 1997, 69–74. DOI: 10.1117/12.271054. URL: https://doi.org/10.1117/12.271054.

[16] Feld, S. A., Loehr, J. P., Sherriff, R. E., Wiemeri, J. and Kaspi, R. In-situ optical monitoring of AlAs wet oxidation using a novel low-temperature low-pressure steam furnace design. *IEEE Photonics Technology Letters* 10.2 (Feb. 1998). DOI: 10.1109/68.655356.

[17] Sakamoto, A., Nakayama, H. and Nakamura, T. Fabrication control during AlAs oxidation of the VCSELs via optical probing technique of AlAs lateral oxidation (OPTALO). *Vertical-Cavity Surface-Emitting Lasers VI*. Ed. by C. Lei and S. P. Kilcoyne. Vol. 4649. International Society for Optics and Photonics. SPIE, 2002, 211–217. DOI: 10.1117/12.469236. URL: https://doi.org/10.1117/12.469236.

[18] *ALOX, Product page, AET Technologies*. Cited 25.10.2020. URL: http://alox.aet-technologies.fr/.

[19] *VIXEL-320, Product specifications, California Scientific, Inc.* Cited 25.10.2020. URL: http://californiascientific.com/products/VIXEL-320_Spec_1906.pdf.

[20] *VF-3000, Product page, Koyo Thermo Systems Co., Ltd.* Cited 25.10.2020. URL: https://www.koyothermos.com/products/semiconductor/vf3000/.

[21] Laaroussi, Y., Chevallier, C., Genty, F., Fressengeas, N., Cerutti, L., Taliercio, T., Gauthier-Lafaye, O., Calmon, P.-F., Reig, B., Jacquet, J. and Almuneau, G. Oxide confinement and high contrast grating mirrors for Mid-infrared VCSELs. *Opt. Mater.*

Express 3.10 (Oct. 2013), 1576–1585. DOI: 10.1364/OME.3.001576. URL: http://www.osapublishing.org/ome/abstract.cfm?URI=ome-3-10-1576.

[22] Lafleur, G., Almuneau, G., Arnoult, A., Camon, H. and Calvez, S. Anisotropy in the wet thermal oxidation of AlGaAs: influence of process parameters. *Opt. Mater. Express* 8.7 (July 2018), 1788–1795. DOI: 10.1364/OME.8.001788. URL: http://www.osapublishing.org/ome/abstract.cfm?URI=ome-8-7-1788.

[23] *HSQ 300, Product specifications, Heraeus Quarzglas GmbH Co. KG*. Cited 30.10.2020. URL: https://www.heraeus.com/media/media/hca/doc_hca/products_and_solutions_8/solids/Solids_HSQ300_330MF_EN.pdf.

[24] Nechay, K., Ulkuniemi, R., Filipchuk, A., Hartikainen, T., Kaivosoja, V., Hietikko, R., Nikkinen, J., Sillanpaa, J., Melanen, P., Vilokkinen, V., Talmila, S. and Uusimaa, P. High-efficiency vertically-emitting chipsets for 3D and proximity sensing. *High-Power Diode Laser Technology XIX*. Ed. by M. S. Zediker. Vol. 11668. International Society for Optics and Photonics. SPIE, 2021, 106–115. DOI: 10.1117/12.2577229. URL: https://doi.org/10.1117/12.2577229.

[25] Calvez, S., Lafleur, G., Arnoult, A., Monmayrant, A., Camon, H. and Almuneau, G. Modelling anisotropic lateral oxidation from circular mesas. *Opt. Mater. Express* 8.7 (July 2018), 1762–1773. DOI: 10.1364/OME.8.001762. URL: http://www.osapublishing.org/ome/abstract.cfm?URI=ome-8-7-1762.

[26] Ko, S.-C., Lee, S. and Chou, Y. Wet Oxidation in a Square Sandwich Composite of GaAs/AlAs/GaAs. *Journal of Electronic Materials - J ELECTRON MATER* 36 (Nov. 2007), 1652–1657. DOI: 10.1007/s11664-007-0265-7.